CrystEngComm

Accepted Manuscript

ROYAL SOCIETY OF CHEMISTRY

www.rsc.org/crystengcomm

Journal Name

RSCPublishing

ARTICLE

Growth and properties of a noncentrosymmetric polyphosphate $CsLa(PO_3)_4$ crystal with deep-ultraviolet transparency

Cite this: DOI: 10.1039/xoxxoooooox

Received ooth January 2012,
Accepted ooth January 2012

DOI: 10.1039/xoxxoooooox

www.rsc.org/

Tongqing Sun,*[a] Pai Shan,[a] Hong Chen,[a] Xuanwen Liu,[b] Hongde Liu,[a] Shaolin Chen,[a] Ya'an Cao,[a] Yongfa Kong[a] and Jingjun Xu[a]

To explore new deep-ultraviolet (deep-UV) nonlinear optical crystals, $CsLa(PO_3)_4$ crystal with noncentrosymmetric crystallographic structure was grown by spontaneous nucleation using the flux method and slow-cooling technique. A single crystal with a size of 28 mm ×14 mm ×5 mm was easily obtained. Two perfect cleavage behaviours of $CsLa(PO_3)_4$ crystal were found and the reason was discussed from the point of view of bond length and symmetry. The thermal stability and specific heat capacity of $CsLa(PO_3)_4$ were investigated. $CsLa(PO_3)_4$ crystal remarkably exhibits a deep-UV cutoff edge of 167nm, which is one of the shortest values among phosphates to date. Polycrystalline powder of $CsLa(PO_3)_4$ presents a moderate second harmonic generation (SHG) response, which is about one half of that of KH_2PO_4 (KDP). The analysis of the dipole moments for the polyhedra and the theoretical calculation by the density functional theory (DFT) were performed for understanding the structure-function relationships in $CsLa(PO_3)_4$ crystal.

Introduction

Deep-ultraviolet (deep-UV) coherent light wavelengths below 200 nm is in increasingly urgent demand in many important applications, such as semiconductor photolithography, laser micromachining, photochemical synthesis, material processing and angle-resolved photoemission spectroscopy with super high resolution.[1–4] The best way to produce deep-UV coherent light with solid-state lasers is through cascaded frequency conversion using deep-UV nonlinear optical (NLO) crystals. However, the exploration of deep-UV NLO materials is a particularly great challenge because of the extremely rigorous prerequisite that includes not only noncentrosymmetric crystallographic structure and considerable chemical stability, but also a rigorous wide band gap (wider than 6.0 eV in order to generate coherent light with wavelength below 200 nm).

Traditionally, the exploration of deep-UV crystals has been mainly focused on beryllium borates because of the following reasons. On one hand, borate compounds have abundant structural units because of the diversity of B and O bonding. On the other hand, based on a theoretical study, beryllium borates possess the largest energy gap among all borates and, hence, the shortest transmission cutoff wavelength in the UV region.[5] Over the past two decades, some noncentrosymmetric beryllium borate crystals that exhibit short transmission cutoff wavelengths in the UV region have been reported, such as $ABe_2BO_3F_2$ (A = Na, K, Rb, Cs, Tl),[6–9] $M_2Be_2B_2O_7$ (M = Sr, Ba),[10, 11] $NaBeB_3O_6$,[12] $ABe_2B_3O_7$ (A = K, Rb),[12] $Na_2CsBe_6B_5O_{15}$,[13] $NaSr_3Be_3B_3O_9F_4$,[14] $NaCaBe_2B_2O_6F$,[15] $Na_2Be_4B_4O_{11}$,[16] $LiNa_5Be_{12}B_{12}O_{33}$,[16] $ReBe_2B_5O_{11}$ (Re = Y, Gd).[17] Among them, KBBF ($KBe_2BO_3F_2$) has been shown to be the best material for deep UV applications and is the only practically usable deep-UV material to date that generates coherent light of wavelength below 200 nm by the direct second harmonic generation (SHG).[18] However, KBBF crystal characterizes a strong growth habit of layering owing to the weak interlayer interactions, which makes it extremely difficult to grow single crystals with large thickness; thus, the coherent light output power is severely limited.[19] Moreover, beryllium (Be) compounds are very poisonous unfortunately. According to the classification of the International Agency for Research on Cancer (IARC), beryllium and beryllium compounds are Category 1 carcinogens.[20, 21] Therefore, it is urgently demanded to develop new and environmentally friendly deep-UV NLO materials.

Recently, two non-beryllium-borate compounds, i.e. $Ba_3P_3O_{10}X$ (X = Cl, Br) were discovered.[22] These two unprecedented phosphates with noncentrosymmetric structures not only display moderate powder SHG intensities in type I phase-matchable behaviors, but also remarkably show short deep-UV cutoff edges (180 nm by $Ba_3P_3O_{10}Cl$ single crystal and <200 nm by polycrystalline $Ba_3P_3O_{10}Br$). Just not long ago, another new phosphate compound with deep-UV transparency, $RbBa_2(PO_3)_5$, was reported.[23] Especially, it shows a large NLO activity of 1.4 × KH_2PO_4 (KDP), which is 2.3 times of that of $Ba_3P_3O_{10}Cl$. The enhanced macroscopic SHG response of $RbBa_2(PO_3)_5$ is attributed to the 1D $[PO_3]_\infty$ chains via corner-sharing of $[PO_4]^{3-}$ tetrahedral units, which exhibit significantly larger microscopic SHG coefficients. Doubtlessly, these discoveries open up a novel and nontoxic field for finding and designing new NLO materials.

The title compound, $CsLa(PO_3)_4$, belongs to the double phosphates of alkali and lanthanide ions with the general formula $ALn(PO_3)_4$, which have been studied extensively for potential applications in the laser technology, catalysis, electricity and optics.[24–28] $CsLa(PO_3)_4$ crystallizes in noncentrosymmetric point

group $C2$ and features 1D $[PO_3]_\infty$ helix chain just as in $RbBa_2(PO_3)_5$, the lately reported deep-UV NLO crystal.[29] It is well known that alkaline and alkaline-earth cations have short absorption edge. The rare-earth caion La^{3+} can also transmit deep-UV light because of its empty 4*f* and 5*d* orbits. So, the likelihood of deep-UV transparency would be expected for $CsLa(PO_3)_4$ crystal. However, the optical property of $CsLa(PO_3)_4$ has not been studied due to the lack of bulk crystal.

Herein, we successfully grew bulk single crystals of $CsLa(PO_3)_4$ and investigated its properties. $CsLa(PO_3)_4$ polycrystalline powder presents a moderate SHG effect (about 0.5 × KDP). Remarkably, the crystal has a UV cutoff edge of 167 nm (one of the shortest values among phosphates to date).

Experimental Section

Crystal growth

$CsLa(PO_3)_4$ crystals were grown by the flux method and slow-cooling technique, and the crystal growth was carried out in a single-zone vertical tubular furnace equipped with a Kanthal AF heater. A SHIMADEN FP21 controller connected to a thyristor was used to control the furnace temperature and the cooling rate.

The starting materials were prepared by mixing of La_2O_3 (4N), Cs_2CO_3 (99.0%) and $NH_4H_2PO_4$ (99.0%) with a molar ratio of 1:5:18 in an agate mortar. These were then transferred into a Φ60 × 60 mm Pt crucible. A stoichiometricLa_2O_3, Cs_2CO_3 and $NH_4H_2PO_4$ generated the title compound, and an excess of Cs_2CO_3 and $NH_4H_2PO_4$ reacted to produce cesium metaphosphate compound, which was served as a self-flux to avoid foreign ions during the crystal growth. Considering the intensive bubbling of NH_3, CO_2, and H_2O, we heated the mixture slowly to be a melt. The melt was homogenized by maintaining at 900 °C until it was clear and there were no bubbles. This process generally lasted about 48hrs due to high viscosity of phosphate melt. The melt was cooled at 5 °C·hr^{-1} till the spontaneous nucleation occurred. At this time there were usually a few of crystal nuclei floating on the melt surface. So the melt temperature was oscillated for reducing the number of nuclei till there was one crystal nucleus left on the surface. Then the crystal was grown by the slow cooling of the melt at a rate of 1 °C per 3 days. Owing to surface tension, the crystal floated on the melt surface. After 15 days, the crystal growth was stopped and the crystal was carefully withdrawn from the melt. It was cooled with the furnace to room temperature at 25 °C·hr^{-1}.

Density and chemical composition

The density of the as-grown $CsLa(PO_3)_4$ crystal at room temperature (23 °C) was measured using a density unit of Sartorius balance (YDK01–C) by the buoyancy method.[30] The chemical composition of the crystal was analyzed by Inductively Coupled Plasm–Atomic Emission Spectrometer (ICP–AES) (Thermo IRIS Advantage).

XRD analysis

The X-ray diffraction (XRD) technique was used to identify the phases of the as-grown crystal and its thermal decomposition products, and to determine the Miller indexes of cleavage planes. The XRD patterns were recorded at room temperature by using a Fangyuan DX2700 (Dandong, China) powder diffractometer with a graphite monochromatized Cu K_α radiation in the 2θ range 10°–70° with a step of 0.02°. An XRD goniometer was used to identify and orientate the crystalline forms that comprised the morphological habit.

Thermal analysis

The thermal stability of $CsLa(PO_3)_4$ was measured by simultaneous Thermogravimetry–Differential Scanning Calorimetry (TG–DSC) method using Netzsch STA 449C in the range 40–1000 °C at 10 °C·min^{-1}. The specific heat capacity was measured using a Mettler-Toledo DSC821^e thermal analyzer in the range 15–90 °C at 10 °C·min^{-1}, and the experiment was run with samples ranging 20–30 mg under atmosphere (benzoic acid was used as the reference substance).

Optical properties

The transmission spectra in the VUV, UV–vis–NIR and mid-far-infrared regions were measured using the VUV station of Beijing Synchrotron Radiation Facility, a Cary 2390 spectrophotometer and a Nicolet Magna-IR560ESP FTIR spectrometer, respectively. A polished $CsLa(PO_3)_4$ crystal was used for measurement, and its optical thickness was 3 mm. The second harmonic response of $CsLa(PO_3)_4$ using the Kurtz-Perry method was evaluated.[31] Small $CsLa(PO_3)_4$ crystals were powdered and graded with standard sieves to obtain a uniform particle size between 15 and 25 μm. The samples was then placed in a 1 mm-thick quartz cell and was irradiated using a pulsed Nd:YAG laser (λ = 1064 nm). The powdered commercial KDP sample sieved into the same size range was used as the standard. The SHG property of a polished crystal was also tested using the same pulsed Nd:YAG laser. SHG efficiency has been shown to depend strongly on particle size, thus the sample of $CsLa(PO_3)_4$ was ground and sieved into several distinct particle size ranges (31–50, 50–76, 76–95, 95–125, 125–180 μm) for further confirming if $CsLa(PO_3)_4$ crystal is phase-matchable.

Computational descriptions

The band structure, density of states (DOS) and dielectric constant of $CsLa(PO_3)_4$ were calculated according to the crystallographic data reported by Sun et al.[29] All calculations were carried out by using the total-energy code CASTEP.[32, 33] The total energy was calculated within the framework of nonlocal gradient-corrected approximations [Perdew-Burke-Ernzerhof (PBE) functional].[34] The interactions between the ionic cores and the electrons were described by the norm-conserving pseudopotential.[35] The following orbital electrons were treated as valence electrons: O-$2s^22p^4$, P-$3s^23p^3$, Cs-$5s^25p^66s^1$ and La-$5d^16s^2$. The number of plane waves included in the basis was determined by a cutoff energy of 1000 eV, and the numerical integration of the Brillouin zone was performed using a 4×3×3 Monkhorst-Pack *k*-point sampling for $CsLa(PO_3)_4$. The other calculating parameters and convergent criteria were the default values of CASTEP code. According to the $(\alpha \cdot h\nu)^{1/2}$–$E_g$ curve (the inset in Fig. 5), a scissor value of 1.78 eV was applied in the subsequent optical property calculations. More than 300 empty bands were used in the optical property calculations. The linear optical properties in terms of the complex dielectric function $\varepsilon(\omega) = \varepsilon_1(\omega) + i\varepsilon_2(\omega)$ were calculated, and optical constants were obtained from the imaginary part of the dielectric function $\varepsilon_2(\omega)$ via the Kramers-Kroning transform.[36]

Results and Discussion

X-ray diffraction

Fig. 1(a) presents an as-grown crystal with a size of 28 mm ×14 mm ×5 mm, which is mostly transparent with a few inclusions in the bottom. The crystal is nonhygroscopic and chemically stable. The

chemical compositions of the as-grown crystal were analysed by ICP–AES, and the results (Table 1) show that the formula of the crystal corresponds to $CsLaP_4O_{12}$.

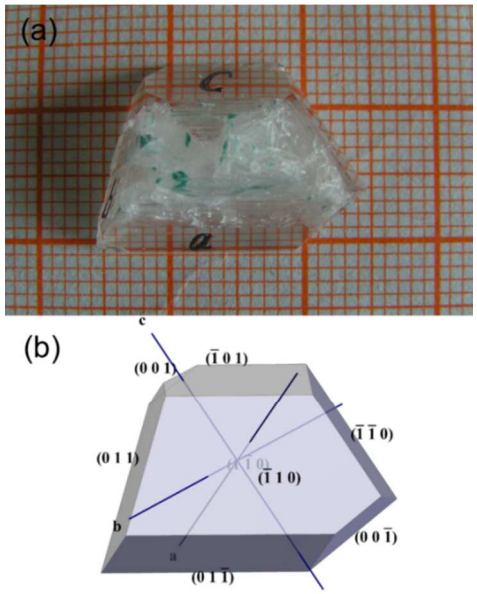

Fig. 1 The photograph (a) of $CsLa(PO_3)_4$ crystal grown by spontaneous nucleation and the stimulated facets (b) marked by Miller indices (hkl).

Table 1 Results of chemical analysis for the as-grown crystal of $CsLa(PO_3)_4$.

Element	Cs (wt%)	La (wt%)	P (wt%)
Calculated	22.6	23.6	21.1
Experimental	23.1	21.6	20.1

Figure 2 shows the XRD pattern of the pulverized $CsLa(PO_3)_4$ crystal. Compared with the standard pattern of $CsLa(PO_3)_4$ (PDF Card No. 97-005-9870), all the diffraction peaks can be indexed with the $P2_1$ symmetry. This confirms that the as-grown crystal has an acentric crystallographic structure. Moreover, no parasitic phases were observed in the pattern, suggesting that pure $CsLa(PO_3)_4$ crystal has been obtained. The cell parameters were calculated from the XRD pattern and the results are a = 7.230 Å, b = 9.283 Å, c = 8.877 Å, β = 99.409, V = 490.7(2) Å^3 and Z = 2. The measured density of the as-grown crystal is 3.28 g·cm^{-3}, which is agreement with the calculated value (3.32 g·cm^{-3}).

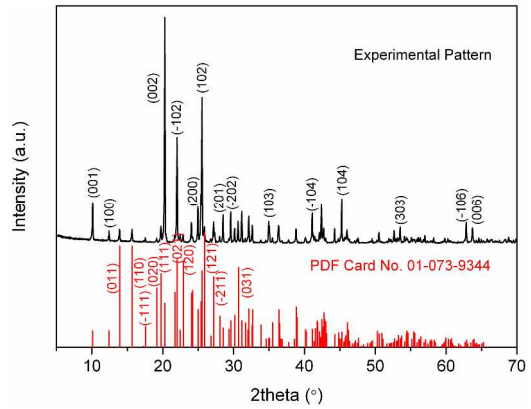

Fig. 2 XRD pattern of $CsLa(PO_3)_4$ observed from pulverized crystal and the standard pattern.

Since the as-grown crystal in Fig. 1(a) presented well-developed facets, the facets were oriented using an X-ray diffraction goniometer. The habit contains crystalline forms {001}, {011}, {$\bar{1}$01}, {110}, etc. The measured interfacial angles among the facets were in good agreement with the calculated angles. The morphology of the as-grown crystal is shown in Fig. 1(b), which was simulated by the WinXMorph software.[37]

Cleavage habit and crystal structure

$CsLa(PO_3)_4$ crystal is very prone to cleavage. When pulverizing a bulk crystal, we noticed the crystal always had fallen to needlelike pieces under external pressure. Though the peak positions of the experiment XRD pattern are consistent with those of the standard pattern, we can see that the intensity differences of the diffraction peaks between the two patterns in Fig. 2 are very distinguishing. This means the seriously preferred orientation existed in the polycrystalline powders prepared from single crystals because of cleavage. Fig. 3 presents two kind of main cleavages for $CsLa(PO_3)_4$ crystals during processing. The cleavage faces were full and smooth, and they were determined to be (100) and (001) crystal planes, respectively.

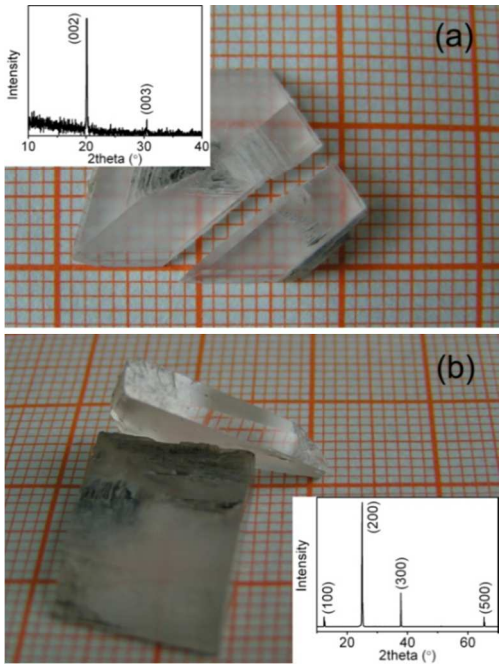

Fig. 3 Typical cleavage behaviors of $CsLa(PO_3)_4$ crystal parallel to (001) (a) and (100) (b). (The insets are the XRD patterns of the cleavage planes.)

The cleavage habit of $CsLa(PO_3)_4$ crystal is related to its structural feature. $CsLa(PO_3)_4$ is characterized by infinite polyphosphate long chains of $[PO_3]_\infty$ consisting of the phosphate units PO_4.[29] The chains run along the [010] direction and are linked along the other two directions, i.e. [100] and [001], by cesium and lanthanum ions through sharing oxygen atoms. Therefore, the structural frame of $CsLa(PO_3)_4$ is formed by intrachain P–O bonds and interchain La–O and Cs–O bonds. The bond valences were calculated according to the Brown and Altermatt parameters.[38] The P–O bonds are much stronger than the La–O and Cs–O bonds according to the values of their bond valences (Table 2). The P–O bonds generate the long chains along the [010] direction, and the interaction between the

chains is weak due to the connection of the La−O and Cs−O bonds. Therefore, we can say that the structure of $CsLa(PO_3)_4$ has the strongest bond strength along the [010] direction. In addition, with respect to the sums of bond valence, Cs^+ and La^{3+} show nonnegligible deviations from their own oxidation numbers, respectively. This means that the oxygen polyhedra of both Cs^+ and $La^{3+}$are not stable. So, the cleavage of $CsLa(PO_3)_4$ crystal easily occurs between the chains, i.e. breaking the weak La−O and Cs−O bonds. As a result, the diffraction peaks of the planes parallel to [010] are remarkably stronger in the experimental XRD pattern than those in the standard one, just as shown in Fig. 2. Contrarily, the peaks of the planes that are not parallel to [010] are usually weaker in the experimental XRD pattern than those in the standard one.

Table 2. The calculated bond valences of La−O, Cs−O and P−O in the structure of $CsLa(PO_3)_4$.

Central atom	Oxidation number	Bond valence	Sum	Deviation
La	+3	0.329~0.502	3.357	11.9%
Cs	+1	0.023~0.181	0.842	−15.8%
P1	+5	1.033~1.480	4.986	−0.3%
P2	+5	1.058~1.460	5.024	0.58%
P3	+5	1.073~1.496	5.191	3.8%
P4	+5	1.025~1.496	5.154	3.1%

Thermal properties

Generally, double phosphate compounds are not stable at high temperatures. To measure its decomposition, a TG−DSC analysis for the $CsLa(PO_3)_4$ crystal was performed. The TG−DSC curves of the $CsLa(PO_3)_4$ crystal are given in Fig. 4. A single sharp endothermic peak is observed at 946 °C, which exhibits the characteristics of a first-order phase transition. The sample weight of $CsLa(PO_3)_4$ does not show representative variation in the measurement temperature up to 1000 °C. A thermal decomposition experiment on $CsLa(PO_3)_4$ was performed at 960 °C in a Muffle oven, and its products was analyzed by XRD. As shown in the inset of Fig. 4, $CsLa(PO_3)_4$ decomposes in accordance with this reaction: $CsLa(PO_3)_4 \longrightarrow LaP_3O_9$ + amorphous phase. This amorphous phase probably contained phosphorus and caesium oxides because the sample weight remained roughly constant.

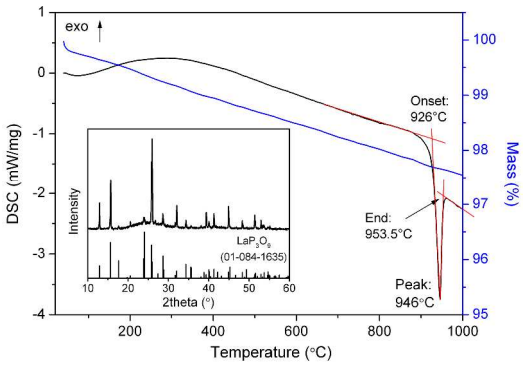

Fig. 4 TG and DSC curves of the $CsLa(PO_3)_4$ crystal. [The inset is the XRD pattern of the thermal decomposition products of $CsLa(PO_3)_4$.]

For nonlinear optical crystals, the damage threshold and possible applications can be greatly influenced by specific heat capacity. The specific heat capacity of $CsLa(PO_3)_4$ was calculated to be 0.513 $J \cdot g^{-1} \cdot K^{-1}$ at 25 °C, which is close to those of other double tetra-metaphosphates crystals, such as $KGd(PO_3)_4$ and $KNd(PO_3)_4$.[39] The corresponding molar heat capacity of $CsLa(PO_3)_4$ is 301.5 $J \cdot mol^{-1} \cdot K^{-1}$.

According to the Dulong-Petit law, at temperatures above the Debye temperature, the molar heat capacity at constant volume C_v of a normal atom is about $3R$ (~25 $J \cdot K^{-1} \cdot mol^{-1}$), where R is the gas constant. But the specific heat of a lighter element such as oxygen is 16.7 $J \cdot K^{-1} \cdot mol^{-1}$, and phosphorus is 22.5 $J \cdot K^{-1} \cdot mol^{-1}$. From the Neumann-Kopp law, the heat capacity of $CsLa(PO_3)_4$ can be determined as a sum of the atomic heat capacities of the component elements, hence the calculated heat capacity of $CsLa(PO_3)_4$ at room temperature is approximately 340.4 $J \cdot K^{-1} \cdot mol^{-1}$. It can be seen that the value of the measured C_p is close to the value of the calculated C_v. Generally speaking, the measured C_p could be considered as C_v because there is little difference between C_p and C_v for a solid substance. The result indicates that the $CsLa(PO_3)_4$ crystal is in accordance with the Dulong-Petit law, and that the Debye temperature of the crystal is higher than room temperature.

Optical properties

Fig. 5 shows the transmission spectra of the $CsLa(PO_3)_4$ crystal. The crystal has not only a high transmittance but also a wide transparency window. The IR cutoff wavelength is around 4 μm because of the absorption resonance of the P−O linkage. The UV cutoff wavelength is as short as 167 nm, that is to say, the band gap of $CsLa(PO_3)_4$ is as large as 7.42 eV. This implies that $CsLa(PO_3)_4$ crystal may have a considerable laser damage threshold. Such a low value of UV cutoff wavelength constitutes one important feature of this crystalline materials, especially when combined with its noncentrosymmetric structure to allow the second and third harmonics of very near-IR beams if possible. The remarkable deep-UV absorption edge of $CsLa(PO_3)_4$ crystal is one of the shortest values among phosphates to date, such as $KTiOPO_4$ (350 nm), $Te_2O(PO_4)_2$ (310 nm by polycrystalline sample), $RbBa_2(PO_3)_5$ (163 nm), $BaP_3O_{10}Cl$ (180 nm) and KDP (an theoretical absorption edge of 176 nm, that is unfortunately unreachable because the unavoidable defects in the crystals that decrease considerably the bandgap).[22, 23, 40, 41] Markedly, such a deep-UV absorption edge is lower than those of most of borate nonlinear crystals, such as CLBO (180 nm), KABO ($K_2Al_2B_2O_7$) (180 nm), and it is also comparable to those of BABF ($BaAlBO_3F_2$, 165 nm) and KBBF (155 nm).[41]

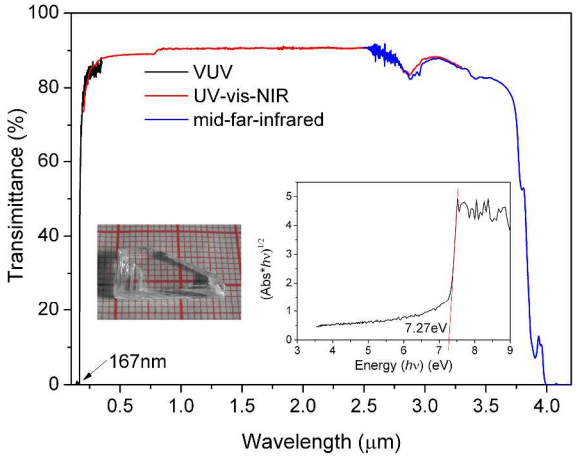

Fig. 5 The transmission spectra of the $CsLa(PO_3)_4$ crystal in the VUV, UV-vis-NIR and mid-far-infrared regions. [The insets presents the photograph of a polished crystal (left) and the indirect energy band gap of $CsLa(PO_3)_4$ (right).]

The powder SHG intensities of $CsLa(PO_3)_4$ and KDP was measured at 1064nm light source by the Kurtz-Perry method. The SHG efficiency of $CsLa(PO_3)_4$ is about half of that of KDP, a widely used NLO crystal. Then a pulsed Nd:YAG laser irradiated a polished $CsLa(PO_3)_4$ crystal (the left inset of Fig. 5) that was randomly rotated for meeting the condition of phase-matching. Unfortunately, no SHG green light of the incident Nd:YAG laser irradiation was observed by naked eyes, which means that $CsLa(PO_3)_4$ crystal could possibly be non-phase-matchable at 1064nm. By sieving the $CsLa(PO_3)_4$ crystal into various particle sizes, ranging from 31 μm to 180 μm, and by measuring the SHG as a function of particle size, we were able to determine the angle phase-matching capability of the material. As shown in Fig. 6, $CsLa(PO_3)_4$ is non-phase-matchable. Based on the SHG efficiency and phase-matching measurements, $CsLa(PO_3)_4$ falls into the Class C category of SHG materials, as defined by Kurtz and Perry.[31]

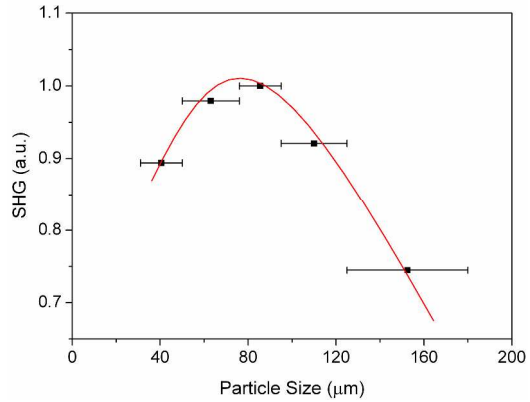

Fig. 6 SHG phase-matching curve, particle size vs SHG efficiency for $CsLa(PO_3)_4$. (The curve drawn is to guide the eye and is not a fit to the data.)

Dipole moment and SHG

Poeppelmeier et al have proposed a method to calculate the local dipole moment of polyhedron by using a bond-valence approaching methodology.[42, 43] The method has been used to better understand the origin of the SHG in some noncentrosymmetric compounds.[44–47] The local dipole moments for the phosphorus tetrahedra and the cesium and potassium polyhedra in $CsLa(PO_3)_4$ were calculated. Table 4 summarizes the direction and magnitude of the dipole moments for the polyhedra in the asymmetric unit of $CsLa(PO_3)_4$. Compared to the PO_4 tetrahedra, the CsO_{10} and LaO_8 have smaller local dipole moments. Especially, the dipole moment of LaO_8 is so weak that it can be neglected. Fig. 7 shows the 1D $[PO_3]_\infty$ helix chain along the *b* axis in $CsLa(PO_3)_4$ and the dipole moments of the PO_4 tetrahedra are also presented. The *x* and *z*-components of their polarization for all the oxygen polyhedra in a unit cell cancel out completely due to the symmetry of 2_1 helical axis, and the *y*-component of their polarization constructively adds to a net value of 19.22 Debye in a unit cell. This value is identical with the result about the foregoing SHG measurement. The net dipole moment in $CsLa(PO_3)_4$ is very much small compared to some compounds with strong SHG response that have been reported recently. For example, $K(VO)_2O_2(IO_3)_3$ crystal has a very large net dipole moment of 129.48 Debye along the *c* axis and consequently exhibits a very strong SHG response of about 36×KDP.[48]

Table 3. Calculation of the dipole moments for the CsO_{10}, LaO_8 and PO_4 polyhedra in $CsLa(PO_3)_4$.

Polar unit	Dipole moment (Debye)			
	x	*y*	*z*	Total magnitude
LaO8	−0.29	−0.33	0.10	0.45
CsO10	0.29	1.46	2.50	2.91
P(1)O4	3.29	1.79	−2.30	4.39
P(2)O4	0.77	4.17	0.51	4.28
P(3)O4	2.47	−1.22	−0.06	2.76
P(4)O4	−0.75	3.74	4.75	6.09

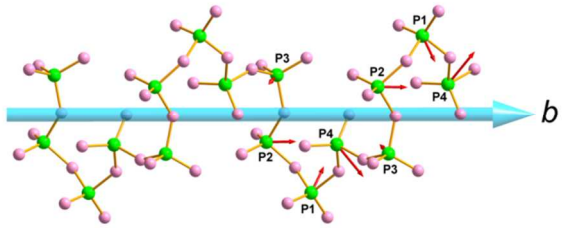

Fig. 7 1D $[PO_3]_\infty$ helix chain along the *b* axis in $CsLa(PO_3)_4$. (The red arrows indicate the approximate direction and magnitude of the dipole moments.)

Theoretical calculation

The calculated band structure of $CsLa(PO_3)_4$ at Brillouin zone was plotted in Fig. 8. The lowest of CBs is localized at the G (0.0, 0.0, 0.0) point with an energy of 5.491 eV. The highest energy of VBs at the B (−0.5, 0.0, 0.0) point is 0.0 eV. Accordingly, we consider the solid-state compound $CsLa(PO_3)_4$ as an insulator with a wide indirect band gap of 5.49 eV. The calculated value of band gap is in principle consistent with the experimental observations (7.42 eV). The obvious DFT underestimation of band gap is associated with the insufficient description of the eigenvalues of the electronic states for the generalized gradient approximation (GGA), especially for insulators.

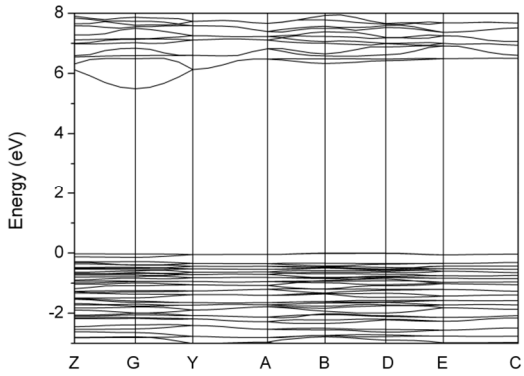

Fig. 8 Band structure of $CsLa(PO_3)_4$.

The total and partial densities of states (TDOS, PDOS) analyses (Fig. 9) indicate that the O-2*p* states make main contributions to the top of VBs near the Fermi level. The VBs from −22.5 to −17.0 eV are predominately composed of the O-2*s* states mixing with minor of Cs-5*s*, P-3*s* and P-3*p* states. The O-2*p* and Cs-5*p* states give rise to the VBs from −11.5 to 0.0 eV. The bands from the bottom of CBs to 15.0 eV mainly result from the unoccupied La-5*d* and P-3*p* states, which means that the La and P atoms act primarily as an electron

donor. Similarly, O atom acts as electron acceptors because their *p* states are localized below E_F.

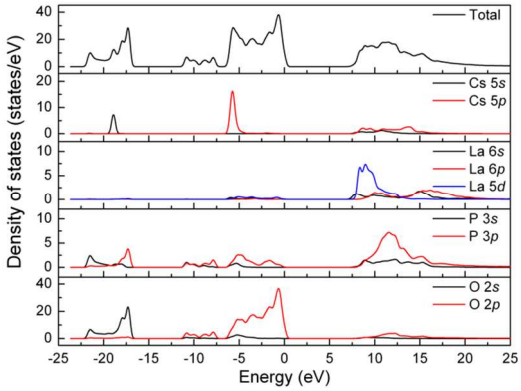

Fig. 9 Total and partial densities of states of $CsLa(PO_3)_4$.

The interband electronic transitions between the occupied and unoccupied states are described by the imaginary part ε_2 (Fig. 10), which indicates that the calculated basic absorption edge is 7.97 eV for $CsLa(PO_3)_4$, in good comparison with the experimental values (7.42 eV). The absorption edge is mainly assigned to the interband electron transitions from O-2*p* state to P-3*p* and La-5*d* states. The average value of the polarized zero-frequency dielectric constants $\varepsilon_1^{ave}(0)$ was calculated to be 2.357 for $CsLa(PO_3)_4$ (Fig. 10).

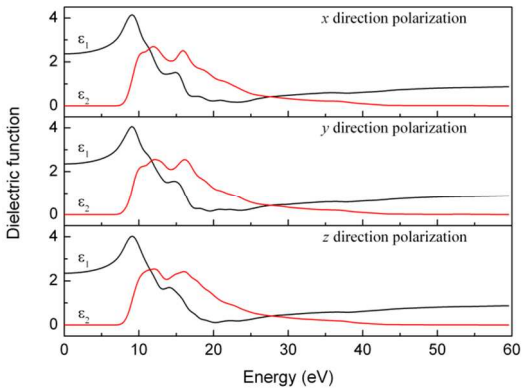

Fig. 10 Energy dependences of the calculated real (ε_1) and imaginary (ε_2) parts of dielectric functions in different polarization directions for $CsLa(PO_3)_4$.

The refractive indexes were also calculated by the relation of $n^2(\omega) = \varepsilon_1(\omega)$, and the energy dependent refractive index curves in different polarization directions is shown in Fig. 11. The average refractive index, defined as $(n_x+n_y+n_z)/3$, was calculated to be 1.5466 at the wavelength of sodium yellow light (λ = 589.3 nm, i.e. 2.1042 eV). The average refractive index of an inorganic mineral can also be calculated via the Gladstone-Dale formula, and the value for $CsLa(PO_3)_4$ is 1.543.[48, 49] These two very close values above show that the calculated results by the DFT theory are reasonable.

The calculated refractive indexes of n_x, n_y and n_z at 1064 nm (i.e. 1.1654 eV) are 1.5424, 1.5381 and 1.5356, respectively. The subsequent birefringence is 0.0068, and this value is rather small among nonlinear optical crystals. The n_x, n_y and n_z at 532 nm (i.e. 2.3308 eV) are 1.5532, 1.5488 and 1.5462, respectively. All of them are higher than those at 1064 nm. This means that $CsLa(PO_3)_4$ crystal cannot realize angle phase-matching of SHG at 1064nm because of its low birefringence. This explains why we have not observed green SHG light on the $CsLa(PO_3)_4$ crystal in the above SHG experiment. A very low birefringence almost means optical isotropy. $CsLa(PO_3)_4$ crystal could be used as window material in the deep-UV range further considering its easily growing and the remarkable deep-UV transparency.

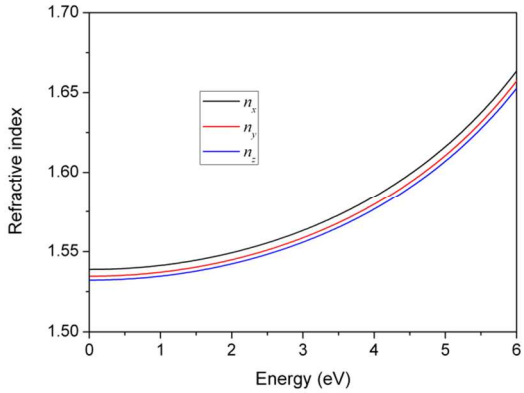

Fig. 11 Variations of the calculated refractive index *n* for $CsLa(PO_3)_4$.

Conclusions

In summary, a centimetre-sized single crystal of $CsLa(PO_3)_4$ was successfully grown by spontaneous nucleation using the flux method and slow-cooling technique. $CsLa(PO_3)_4$ crystal is nonhygroscopic, chemically stable and easily-obtained. The crystal is prone to cleavage parallel to the *b* axis owing to its structural character, which makes it easily processed. The compound has good thermal stability to 926 °C and its specific heat capacity is 0.513 $J \cdot g^{-1} \cdot K^{-1}$ at 25 °C. Remarkably, $CsLa(PO_3)_4$ crystal exhibits a UV cutoff edge of 167 nm, which is one of the shortest values among phosphates to date. Polycrystalline $CsLa(PO_3)_4$ powder presents a moderate SHG response about 1/2 times of that of KDP. Though the crystal cannot realize angle phase-matching of SHG because of its very low birefringence, it is still doubtless that phosphate would be as a novel and promising field for the future exploration of deep-UV NLO materials.

Acknowledgements

This work was supported by the National Natural Science Foundation of China (Grant No. 21271109) and the Fundamental Research Funds for the Central Universities of China (Grant No. 65122011).We thank Prof. Ye Tao (VUV station of Beijing Synchrotron Radiation Facility, Institute of High Energy Physics, Chinese Academy of Sciences) for measuring the VUV transmission spectrum and Dr. Shifeng Jin (Institute of Physics, Chinese Academy of Science) for his help in measuring the SHG phase-matching curve.

Notes and references

[a] The MOE Key Laboratory of Weak-Light Nonlinear Photonics and School of Physics, Nankai University, Tianjin 300071, P. R. China. Fax: +86-22-23501594; Tel: +86-22-23506257; E-mail: suntq@nankai.du.cn.
[b] School of Resources and Materials, Northeastern University at Qinhuangdao, Qinhuangdao 066004, P. R. China.

1. Y.N. Xia, C.T. Chen, D.Y. Tang and B.C. Wu, *Adv. Mater.*, 1995, **7**, 79.

2. J.Q. Meng, G.D. Liu, W.T. Zhang, L. Zhao, H.Y. Liu, X.W. Jia, D.X. Mu, S.Y. Liu, X.L. Dong, J. Zhang, W. Lu, G.L. Wang, Y. Zhou, Y. Zhu, X.Y. Wang, Z.Y. Xu, C.T. Chen and X.J. Zhou, *Nature* 2009, **462**, 335.
3. H.P. Wu, H.W. Yu, Z.H. Yang, X.L. Hou, X. Su, S.L. Pan, K.R. Poeppelmeier and J.M. Rondinelli, *J. Am. Chem. Soc.*, 2013, **135**, 4215.
4. S.G. Zhao, P.F. Gong, L. Bai, X. Xu, S.Q. Zhang, Z.H. Sun, Z.S. Lin, M.C. Hong, C.T. Chen and J.H. Luo, *Nat. Commun.*, 2014, **5**, 4019.
5. R.K. Li, *J. Non-Cryst. Solids*, 1989, **111**, 199.
6. L.F. Mei, Y.B. Wang and C.T. Chen, *Mater. Res. Bull.*, 1994, **29**, 81.
7. L. Mei, X. Huang, Q. Wu, B. Wu and C.Z. Chen, *Kristallogr.* 1995, **210**, 93.
8. C.T. Chen, S.Y. Luo, X.Y. Wang, G.L. Wang, X.H. Wen, H.X. Wu, X. Zhang and Z.Y. Xu, *J. Opt. Soc. Am. B*, 2009, **26**, 1519.
9. C.D. McMillen, J. Hu, D.V. Derveer and J.W. Kolis, *Acta Crystallogr. B* 2009, **65**, 445.
10. C.T. Chen, Y.B. Wang, B.C. Wu, K.C. Wu, W.L. Zeng and L.H. Yu, *Nature* 1995, **373**, 322.
11. H. Qi and C.T. Chen, *Inorg. Chem. Commun.*, 2001, **4**, 565.
12. S.C. Wang, N. Ye, W. Li and D. Zhao, *J. Am. Chem. Soc.*, 2010, **132**, 8779.
13. S.C. Wang and N. Ye, *J. Am. Chem. Soc.*, 2011, **133**, 11458.
14. H.W. Huang, J.Y. Yao, Z.S. Lin, X.Y. Wang, R. He, W.J. Yao, N.X. Zhai and C.T. Chen, *Angew. Chem. Int. Ed.*, 2011, **50**, 9141.
15. H.W. Huang, J.Y. Yao, Z.S. Lin, X.Y. Wang, R. He, W.J. Yao, N.X. Zhai and C.T. Chen, *Chem. Mater.*, 2011, **23**, 5457.
16. H.W. Huang, L.J. Liu, S.F. Jin, W.J. Yao, Y.H. Zhang and C.T. Chen, *J. Am. Chem. Soc.*, 2013, **135**, 18319.
17. X. Yan, S.Y. Luo, Z.S. Lin, J.Y. Yao, R. He, Y.C. Yue and C.T. Chen, *Inorg. Chem.*, 2014, **53**, 1952.
18. C.T. Chen, G.L. Wang, X.Y. Wang and Z.Y. Xu, *Appl. Phys. B: Lasers Opt.*, 2009, **97**, 9.
19. H.P. Wu, H.W. Yu, S.L. Pan, Z.J. Huang, Z.H. Yang, X. Su and K.R. Poeppelmeier, *Angew. Chem. Int. Ed.*, 2013, **52**, 3406.
20. IARC Monograhs on the Evaluation of Carcinogenic Risks to Humans International Agency for Research on Cancer, 1993, Vol. 58, pp 377.
21. R. Puchta, *Nat. Chem.*, 2011, **3**, 416.
22. P. Yu, L.M. Wu, L.J. Zhou and L. Chen, *J. Am. Chem. Soc.*, 2014, **136**, 480.
23. S.G. Zhao, P.F. Gong, S.Y. Luo, L. Bai, Z.S. Lin, C.M. Ji, T.L. Chen, M.C. Hong and J. H. Luo, *J. Am. Chem. Soc.*, 2014, **136**, 8560.
24. H. Ettis, H. Naïli and T. Mhiri, *Cryst. Growth Des.*, 2003, **3**, 599.
25. I. Parreu, J.J. Carvajal, X. Solans, F. Díaz and M. Aguiló, *Chem. Mater.*, 2006, **18**, 221.
26. I. Parreu, R. Solé, J. Massons, F. Díaz and M. Aguiló, *Cryst. Growth Des.*, 2007, **7**, 557.
27. I. Parreu, M.C. Pujol, M. Aguiló, F. Díaz, X. Mateos and V. Petrov, *Opt. Express* 2007, **15**, 2360.
28. T.Q. Sun, Y. Zhang, P. Shan, Z.C. Zhang, S.L. Chen, Y.F. Kong and J.J. Xu, *PLOS ONE* 2014, **9**, e100922.
29. T.Q. Sun, G.Q. Shen, X.Q. Wang, R.J. Wang, J.Z. Wei and D.Z. Shen, *Acta Crystallogr. E*, 2004, **60**, i28.
30. W.G. Zhang, P.S. Halasyamani, Z.L. Gao, S.P. Wang, J. Wang and X.T. Tao, *Cryst. Growth Des.*, 2011, **11**, 3636.
31. S.K. Kurtz and T.T. Perry, *J. Appl. Phys.*, 1968, **39**, 3798.
32. M.D. Segall, P.L.D. Lindan, M.J. Probert, C.J. Pickard, P.J. Hasnip, S.J. Clark and M.C.J. Payne, *Phys.: Cond. Matt.*, 2002, **14**, 2717.
33. V. Milman, B. Winkler, J.A. White, C.J. Pickard, M.C. Payne, E.V. Akhmatskaya and R.H. Nobes, *Int. J. Quantum Chem.*, 2000, **77**, 895.
34. J.P. Perdew, K. Burke and M. Ernzerhof, *Phys. Rev. Lett.*, 1996, **77**, 3865.
35. J.S. Lin, A Qteish, M.C. Payne and V. Heine, *Phys. Rev. B*, 1993, **47**, 4174.
36. J.R. Macdonald and M.K. Brachman, *Rev. Mod. Phys.*, 1956, **28**, 393.
37. W. Kaminsky, *J. Appl. Crystallogr.*, 2007, **40**, 382-385.
38. I. D. Brown and D. Altermatt, *Acta Crystallogr. B*, 1985, **41**, 244.
39. T.Q. Sun, X.D. Zhou, X.Q. Wang, G.Q. Shen, Y.F. Kong, J.J. Xu and D.Z. Shen, *J. Cryst. Growth*, 2010, **312**, 1627.
40. M.K. Kim, S.H. Kim, H.Y. Chang, P.S. Halasyamani and K.M. Ok, *Inorg. Chem.*, 2010, **49**, 7028.
41. D.N. Nikogosyan, *Nonlinear optical crystals: a complete survey*, Springer Press: New York, 2005, pp 64-269.
42. P.A. Maggard, T.S. Nault, C.L. Stern and K.R. Poeppelmeier, *J. Solid State Chem.*, 2003, **175**, 27.
43. H.K. Izumi, J.E. Kirsch, C.L. Stern and K.R. Poeppelmeier, *Inorg. Chem.*, 2005, **44**, 884.
44. K.M. Ok and P.S. Halasyamani, *Inorg. Chem.*, 2005, **44**, 3919.
45. H.Y. Chang, S.W. Kim and P.S. Halasyamani, *Chem. Mater.*, 2010, **22**, 3241.
46. S.G. Zhao, X.X. Jiang, R He, S.Q. Zhang, Z.H. Sun, J.H. Luo, Z.S. Lin and M. C. Hong, *J. Mater. Chem. C*, 2013, **1**, 2906.
47. C.F. Sun, C.L. Hu, X. Xu, B.P. Yang and J.G. Mao, *J. Am. Chem. Soc.*, 2011, **133**, 5561.
48. J.A. Mandarino, *Can. Mineral.*, 1976, **14**, 498.
49. D.N. Ye, *Structural and optical mineralogy*, Geology Press: Beijing, 1988, pp 18-26.

Growth and properties of a noncentrosymmetric polyphosphate $CsLa(PO_3)_4$ crystal with deep-ultraviolet transparency

Tongqing Sun,*[a] Pai Shan,[a] Hong Chen,[a] Xuanwen Liu,[b] Hongde Liu,[a] Shaolin Chen,[a] Ya'an Cao,[a] Yongfa Kong[a] and Jingjun Xu[a]

[a] The MOE Key Laboratory of Weak-Light Nonlinear Photonics and School of Physics, Nankai University, Tianjin 300071, P. R. China.

[b] School of Resources and Materials, Northeastern University at Qinhuangdao, Qinhuangdao 066004, P. R. China.

Single crystal of $CsLa(PO_3)_4$ has been successfully grown, and it exhibits a remarkable deep-UV cutoff edge of 167nm.